analytical chemistry

pubs.acs.org/ac Article

Ultrathin Graphdiyne/Graphene Heterostructure as a Robust Electrochemical Sensing Platform

Xiuchao Sun, Menglu Duan, Rongteng Li, Yuan Meng, Qiang Bai, Lina Wang,* Manhong Liu, Zhugen Yang, Zhiling Zhu,* and Ning Sui*

Cite This: *Anal. Chem.* 2022, 94, 13598−13606 Read Online

ACCESS | Metrics & More | Article Recommendations | Supporting Information

ABSTRACT: Graphdiyne (GDY) has been considered as an appealing electrode material for electrochemical sensing because of its alkyne-rich structure and high degrees of π-conjugation, which shows great affinity to heavy metal ions and pollutant molecules via d−π and π−π interactions. However, the low surface area and poor conductivity of bulk GDY limit its electrochemical performance. Herein, a two-dimensional ultrathin GDY/graphene (GDY/G) nanostructure was synthesized and used as an electrode material for electrochemical sensing. Graphene plays the role of an epitaxy template for few-layered GDY growth and conductive layers. The formed few-layered GDY with a high surface area possesses abundant affinity sites toward heavy metal ions (Cd^{2+}, Pb^{2+}) and toxic molecules, for example, nitrobenzene and 4-nitrophenol, via d−π and π−π interactions, respectively. Moreover, hemin as a key part of the enzyme catalytic motif was immobilized on GDY/G via π−π interactions. The artificial enzyme mimic hemin/GDY/G-modified electrode exhibited promising ascorbic acid and uric acid detection performance with excellent sensitivity and selectivity, a good linear range, and reproducibility. More importantly, real sample detection and the feasibility of this electrochemical sensor as a wearable biosensor were demonstrated.

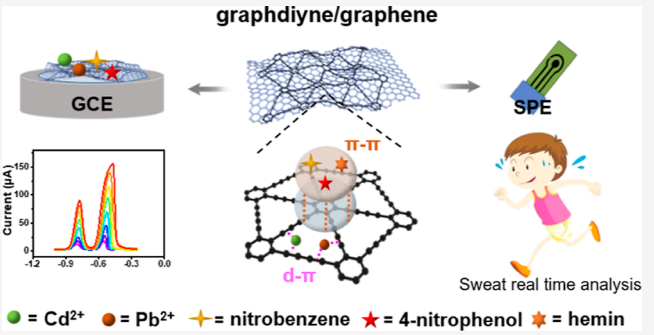

1. INTRODUCTION

Due to the high sensitivity, fast response time, and wide detection range of electrochemical sensors, they have been widely used in the fields of disease detection,[1−3] environmental monitoring,[4,5] drug screening,[6,7] and so forth. The electrode material plays an important role in electrochemical sensors as it can affect the detection in terms of the rate of heterogeneous electron transfer (e.g., response time), the double-layer capacitance (e.g., limit of detection), and the nature of the coupling chemistry. The electrode material plays the role of selectively interacting with the analyte and converting the result into electrochemical signals; thus, an electrode material with high selectivity and high conductivity is the preferred material for electrochemical sensors. To pursue a high sensitivity, a nanomaterial is regarded as a promising electrode material because it has a high surface area, which can increase the active electrode area since the Faradaic current depends directly on the active area of the electrode. Nowadays, many electrode materials have been developed, including noble metal nanostructures,[8] carbon materials,[9] metal oxide nanostructures,[10] and so forth. Although a noble metal nanostructure is regarded as a high-activity electrode material in electrochemical sensing, it has the disadvantages of poor stability, high cost, and a complex preparation process, which restrict its application. The poor conductivity of metal oxide nanostructures has become an obstacle in the application as electrode materials, and a material with high conductivity is always combined to improve the conductivity of the electrode, such as graphene. Dau et al. loaded Fe_3O_4 onto graphene and increased the response current by a factor of 20.[11] A carbon nanostructure shows high stability, low cost, excellent conductivity, and facile surface functionalization and is regarded as a promising electrode material for electrochemical sensors, such as graphene,[12] carbon nanotubes,[13] active carbon,[14] GDY,[15] and so forth.

GDY is a new member of carbon allotropes with two-dimensional (2D) layers. Each hexagonal benzene ring is bridged by six alkynyl linkages (−C≡C−C≡C−), and the carbon atoms are hybridized in the forms of sp and sp^2. The unique structure endows GDY with fascinating properties, such as highly conjugated π-electronic structures, abundant chemical bonds, highly carrier mobility, and stability.[16] Plenty of well-defined GDY nanostructures including 0D nano-

Received: August 4, 2022
Accepted: September 9, 2022
Published: September 20, 2022

https://doi.org/10.1021/acs.analchem.2c03387
Anal. Chem. 2022, 94, 13598−13606

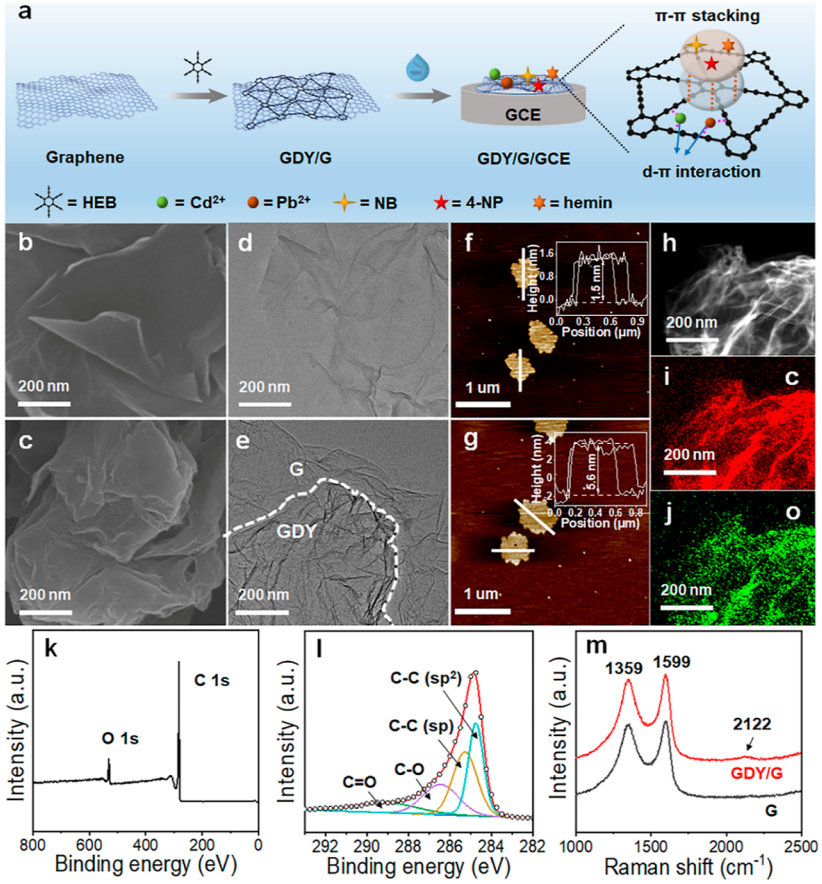

Figure 1. (a) Schematic illustration of the preparation of the GDY/G heterostructure and its application in the detection of heavy metal ions (Cd^{2+}, Pb^{2+}) and toxic molecules (NB, 4-NP). (b–g) SEM, TEM, and AFM images of (b,d,f) graphene and (c,e,g) GDY/G. (h–j) STEM image and EDS elemental maps of GDY/G for (i) C and (j) O elements. (k) XPS survey spectra of GDY/G. (l) XPS C 1s spectrum of GDY/G. (m) Raman shift of graphene and GDY/G.

particles,[17] 1D nanowires,[18] 2D nanosheets,[19] and 3D structures were reported.[20] These GDY structures were used as electrode materials in versatile electrochemical sensing. Li et al. reported a GDY powder-modified electrode that presents high sensitivity for metal ion detection[21] due to the high affinity between metal ions and alkynyl bonds. Niu et al. reported a nitrogen-doped GDY powder as an electrode material for the detection of environment pollutants.[22] The doping of N atoms can enhance the electrical conductivity, which improves its electrochemical sensing performance. 2D nanostructures attract tremendous attention because of their anisotropic morphology and greatly expanded surface area with the exposure of more active sites, endowing the electrode with ultrahigh surface sensitivity to the environment. The development of few-layered GDY 2D nanostructures is expected to improve the electrochemical activity. However, few electrochemical sensors were reported based on few-layered GDY as the electrode material since the synthesis of such few-layered GDY remains challenging.

In this study, few-layered GDY was synthesized by using liquid-exfoliated graphene as an epitaxy template. Moreover, the presence of graphene significantly enhances the conductivity of GDY/G heterostructures, which can improve the performance of electrochemical sensing. GDY shows great affinity to metal ions (via d–π conjugation due to the presence of C≡C) and molecules consisting of π-electronic structures (via π–π attraction due to highly conjugated π-electronic structures of GDY). The GDY/G modified electrode was demonstrated as an efficient electrochemical sensor; it shows high sensitivity for heavy metal ions (Cd^{2+}, Pb^{2+}) and toxic molecules [nitrobenzene (NB), 4-nitrophenol (4-NP)]. Hemin as a key part of the enzyme catalytic motif was immobilized on GDY/G via π–π interactions. Its electrochemical sensing performance is enhanced by using GDY/G as a support. Hemin/GDY/G was successfully used for ascorbic acid (AA) and uric acid (UA) detection. In all, GDY/G is evidenced to be an efficient electrode material to improve the electrochemical sensing, which holds a wide spectrum of applications in environmental monitoring and biomedical diagnosis.

2. EXPERIMENTS

2.1. Chemicals and Materials. Cadmium nitrate tetrahydrate ($Cd(NO_3)_2{\cdot}4H_2O$, 99%), lead(II) nitrate ($Pb(NO_3)_2$, ≥99%), 4-NP (≥99%), and NB (≥99.7%) were purchased from Aladdin Chemical Reagent Co., Ltd. AA (≥99.7%) was purchased from Sinopharm Chemical Reagent Co., Ltd. UA (98%) was purchased from Shanghai Macklin Biochemical Co., Ltd. (Shanghai, China). All chemicals were not further purified before use. Ultrapure water (18.25 MΩ·cm) was prepared using a Milli-Q system (USA).

2.2. Synthesis of GDY/G. GDY/G was synthesized from our previous work.[23] Tetrabutylammonium fluoride (1 M in THF, 1 mL) was added into a solution of 100 mg of hexakis[(trimethylsilyl)-ethynyl]benzene (HEB–TMS) and 40

https://doi.org/10.1021/acs.analchem.2c03387
Anal. Chem. 2022, 94, 13598–13606

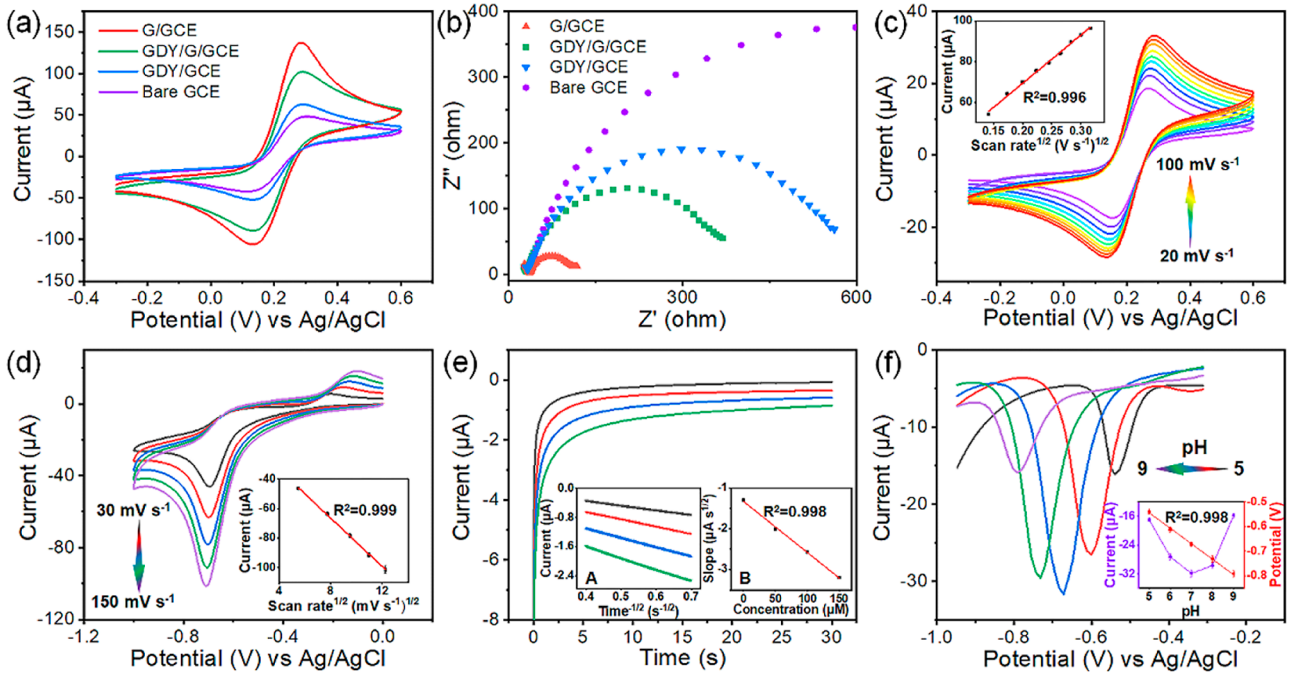

Figure 2. (a) CV curves and (b) EIS of bare GCE, G/GCE, GDY/GCE, and GDY/G/GCE in 5.0 mM $[Fe(CN)_6]^{3-/4-}$ solution containing 0.1 M KCl. (c) CV curves of GDY/G/GCE in 5.0 mM $[Fe(CN)_6]^{3-/4-}$ solution containing 0.1 M KCl at different scan rates. Inset: linear relationship between the anodic peak currents and the square root of scan rate. (d) CV curves obtained at different scan rates for GDY/G/GCE aimed at the reduction of 200 μM NB in pH 7.0. Inset: linear relationship between the peak currents and the square root of scan rate. (e) Chronoamperometric response at GDY/G/GCE in pH 7.0 with different concentrations of NB: 0, 50, 100, and 150 μM. Inset A: linear relationship between the peak current (I) and $t^{-1/2}$ derived from the chronoamperogram data. Inset B: dependence of the slope of the straight lines against the NB concentrations. (f) DPV curves of 200 μM NB at GDY/G/GCE in 0.1 M PBS with different pH values (5.0, 6.0, 7.0, 8.0, and 9.0). The inset shows the dual plots of peak current and potential vs pH.

mL of dichloromethane (DCM) and stirred at 0 °C for 15 min. Then, the mixture was washed with deionized water, dried by anhydrous $MgSO_4$, and filtered. The precursor HEB was added dropwise into a three-necked flask containing a 40 mL pyridine solution of mixed 10 mg of graphene and 50 mg of $Cu(OAc)_2$. The mixture was then kept at room temperature in the dark under an argon atmosphere for 1 day. The solid product was collected by centrifugation and washed with pyridine, DMF, 1 M HCl, and ultrapure water. Finally, the precipitate was freeze-dried to obtain the final product GDY/G.

2.3. Preparation of the Modified Electrode. Before the modification, a glassy carbon electrode (GCE) of 3 mm diameter was cleaned by polish with 0.3 and 0.05 μm alumina slurries and then rinsed with ethanol and ultrapure water to get a fresh surface to use. 5 mg of GDY/G was dispersed into 1 mL of equal volume ultrapure water, ethanol, and 0.5 wt % Nafion solution, and it was uniformly dispersed after ultrasonic treatment. Then 5 μL of the homogeneous solution was dropped on the GCE surface and dried in the air to get the GDY/G-modified electrode.

2.4. Electrochemical Measurements. Electrochemical determination was carried out with a CHI-660E electrochemical workstation (Shanghai Chenhua Instruments Limited, China). A standard three-electrode cell was used for the electrochemical experiments. The Ag/AgCl (3 M KCl) electrode, modified GCE, and the platinum wire electrode were used as the reference, working, and counter electrodes, respectively. According to the definition of International Union of Pure and Applied Chemistry (IUPAC), the estimation formula of the limit of detection (LOD) is

$$\mathrm{LOD} = K \times S_b/m \quad (1)$$

where S_b is the standard deviation (SD) of the reaction of the blank solution (without the analyte), m is the slope of the analyte in the linear detection range, and K is a numerical factor selected based on the expected confidence level ($K = 3$ is used, allowing a confidence level of 99.86%).

3. RESULTS AND DISCUSSION

3.1. Morphological and Structural Characterization. Figure 1a illustrates the preparation process of the GDY/G heterostructure. The ultrathin GDY/G heterostructure was constructed using graphene as a structure guiding template. Due to lattice match and the van der Waals interaction between GDY and graphene, GDY film was easy to grow on the surface of graphene.[24,25] The morphology of the product was analyzed by scanning electron microscopy (SEM) (Figure 1b,c). Compared with pristine graphene, the surface of graphene is rough after GDY growth. The transmission electron microscopy (TEM) image confirms that GDY/G is a lamellar structure, consistent with the morphology of graphene sheets, indicating that GDY grows in planes on graphene (Figure 1d,e). In comparison, GDY was prepared in the same way but without graphene as a template; a 3D amorphous structure was obtained (Figure S1). Atomic force microscopy (AFM) shows that graphene and GDY/G have thin thicknesses of 1.5 and 5.6 nm, respectively (Figure 1f,g). In Figure 1h−k, energy-dispersive spectroscopy (EDS) elemental mapping and X-ray photoelectron spectroscopy (XPS) images imply that GDY/G consisted mainly of carbon, which is uniformly distributed throughout the film. The

https://doi.org/10.1021/acs.analchem.2c03387
Anal. Chem. 2022, 94, 13598−13606

presence of oxygen may be due to adsorption of oxygen from the air or unavoidable defects.[26] The C 1s spectrum can be deconvoluted into four peaks belonging to the C═C, C≡C, C−O, and C═O bonds (Figure 1l).[25] Figure 1m shows the Raman spectra of graphene and GDY/G. In the Raman spectra of graphene, the peaks located at 1348 and 1601 cm^{-1} correspond to the D- and G-bands, respectively.[23,27] In the Raman spectra of GDY/G, the peaks located at 1359 and 1599 cm^{-1} are graphene lattice vibrations, and 2122 cm^{-1} can be attributed to the C≡C bond vibrations of GDY.[23,28]

3.2. Electrochemical Characterization of Modified Electrodes. By using cyclic voltammetry (CV), the electrochemical behavior of different electrodes was studied (Figure 2a). Since graphene nanosheets can speed up the diffusion of $[Fe(CN)_6]^{3-/4-}$ onto the surface of the electrode, G/GCE exhibits the highest peak current. Nevertheless, owing to the low conductivity of bulk GDY, the peak current significantly drops after modification with GDY (i.e., GDY/GCE). When compared to GDY/GCE, the peak current for GDY/G/GCE shows a significant improvement, proving that graphene can facilitate efficient electron transfer on the electrode surface and increase electrochemical activity.[29−31]

Electrochemical impedance spectroscopy (EIS) is frequently used to study the characteristics of electrode interfaces.[32−34] The Nyquist plots of four modified electrodes are displayed in Figures 2b and S2. The smallest semicircle diameter at high frequency is seen in G/GCE, indicating the lowest charge-transfer resistance (R_{ct}). The semicircle diameter clearly increases in the case of GDY/GCE, showing an increased R_{ct} of bulk GDY. Interestingly, compared to GDY/GCE, the relevant R_{ct} value drops when GDY is incorporated into graphene. The obvious decrease could be attributed to the addition of conductive graphene, which can reduce the impedance barrier for mass and charge transfer at the electrode surface.

The real electrochemical active surface areas have a great influence on electrochemical behavior.[29,35] By using CV at various scan rates, the electrochemical surface areas of GDY/G/GCE (Figure 2c) were investigated. It is evident that as the square root of the scan rate increases, the anodic peak current grows linearly. The linear equation can be determined: $I(A) = 2.37 \times 10^{-4} \nu^{1/2} + 2.18 \times 10^{-5}$. As a result, the Randles−Sevcik equation can be used to calculate the electrochemical surface areas[30,36]

$$I = (2.69 \times 10^5) n^{3/2} A C D^{1/2} \nu^{1/2} \quad (2)$$

where I is the anodic peak current (A), ν is the scan rate (V s^{-1}), A is the effective surface area of the working electrode (cm^2), C is the concentration of the electroactive species (mol cm^{-3}), D is the diffusion coefficient of $[Fe(CN)_6]^{3-/4-}$ equal to 7.60×10^{-7} cm^2 s^{-1}, and n is the number of transferred electrons. For comparison, the electrochemical active surface areas of bare GCE, G/GCE, and GDY/GCE were studied under the same conditions (Figure S3). The results show that the electrochemical active surface areas of G/GCE, GDY/GCE, GDY/G/GCE, and bare GCE were 0.109, 0.042, 0.064, and 0.026 cm^2, respectively. In other words, the ultrathin 2D GDY/G heterostructure is expected to enhance electrochemical behavior with high peak currents, a smooth electron-transfer process, and a large electrochemical active surface area. These results confirm that GDY/G/GCE provides a platform for the construction of electrochemical sensors.

3.3. Optimization of Experimental Parameters. GDY/G heterostructures with different ratios were prepared by changing the amount of HEB (50, 75, 100, 125, and 150 mg). As shown in Figure S4, when HEB was added at 100 mg, the current reached the maximum value. When the amount of HEB increased, the thickness of the GDY layer increased and the conductivity of the GDY/G heterostructure decreased because the contribution of graphene to the conductivity of the heterostructure is diminished by the excessively thick GDY layer. The peak current also decreases when the HEB content is below 100 mg, which may be due to the discontinuity of the GDY layer loaded on graphene, resulting in fewer adsorption sites. These results indicate that graphene is not only a template to ensure the synthesis of few-layered GDY but also a cornerstone for the conductivity of the GDY/G heterostructure.

The possible influence of scan rate toward NB reduction at GDY/G/GCE was studied by CV (Figure 2d). The reduction peak current increases linearly with the increase of the square root of scan rate (R^2 = 0.999). This shows that the electrochemical reduction of NB on the modified electrode is driven by a normal diffusion-controlled process. The diffusion coefficient of the electrochemical process on the electrode surface was studied using the chronoamperometry method (Figure 2e). The diffusion coefficient can be calculated from Cottrell's equation in the diffusion control process[37]

$$I = nFAD^{1/2} C \pi^{-1/2} t^{-1/2} \quad (3)$$

where D is the diffusion coefficient (cm^2 s^{-1}) and C is the bulk concentration (mol cm^{-3}). Inset A of Figure 2e shows that $t^{-1/2}$ is linear with the peak current. The concentration of NB is also linear to the slopes in inset A (inset B of Figure 2e). The diffusion coefficient of NB is calculated to be 7.033×10^{-6} cm^2 s^{-1}, according to Cottrell's equation.

When multiple protons are involved in the redox process, the acidity of the detected substance affects the mass transport rate of the electrode surface.[38−40] The effects of pH on the redox current responses and potentials for GDY/G/GCE toward NB were investigated by differential pulse voltammetry (DPV) in PBS at pH values from 5.0 to 9.0 (Figure 2f). The response current increases gradually with pH increasing from 5.0 to 7.0 but then decreases with a further increase of pH value. Hence, pH 7.0 is regarded as the optimum pH for NB detection. In addition, with the increase of pH, the reduction potential shifted negatively, indicating that protons were involved in the charge-transfer process.[33] The inset of Figure 2f shows that the reduction potential (E_p) changes linearly with increasing pH. The equation is $E_p(V) = -0.0627$ pH—0.231 (R^2 = 0.998). The slope of 62.7 mV pH^{-1} is close to the theoretical value of 59 mV pH^{-1}, indicating that the number of protons and electrons transferred during NB reduction is equal.[37,41]

3.4. Electrochemical Detection of NB on Different Modified Electrodes. The effects of different modified GCEs on the electrochemical detection of NB were studied by DPV. As shown in Figure S5, bare GCE displays the lowest peak currents. For GDY and graphene-modified GCE, the reduction peak current is significantly enhanced, compared with bare GCE, which can be attributed to the high affinity of graphene and GDY for NB. In addition, the reduction peak current of GDY/GCE is greater than that of G/GCE, which proves that GDY has a stronger affinity for NB than graphene. Specifically, among the investigated four electrodes, GDY/G/GCE

https://doi.org/10.1021/acs.analchem.2c03387
Anal. Chem. 2022, 94, 13598−13606

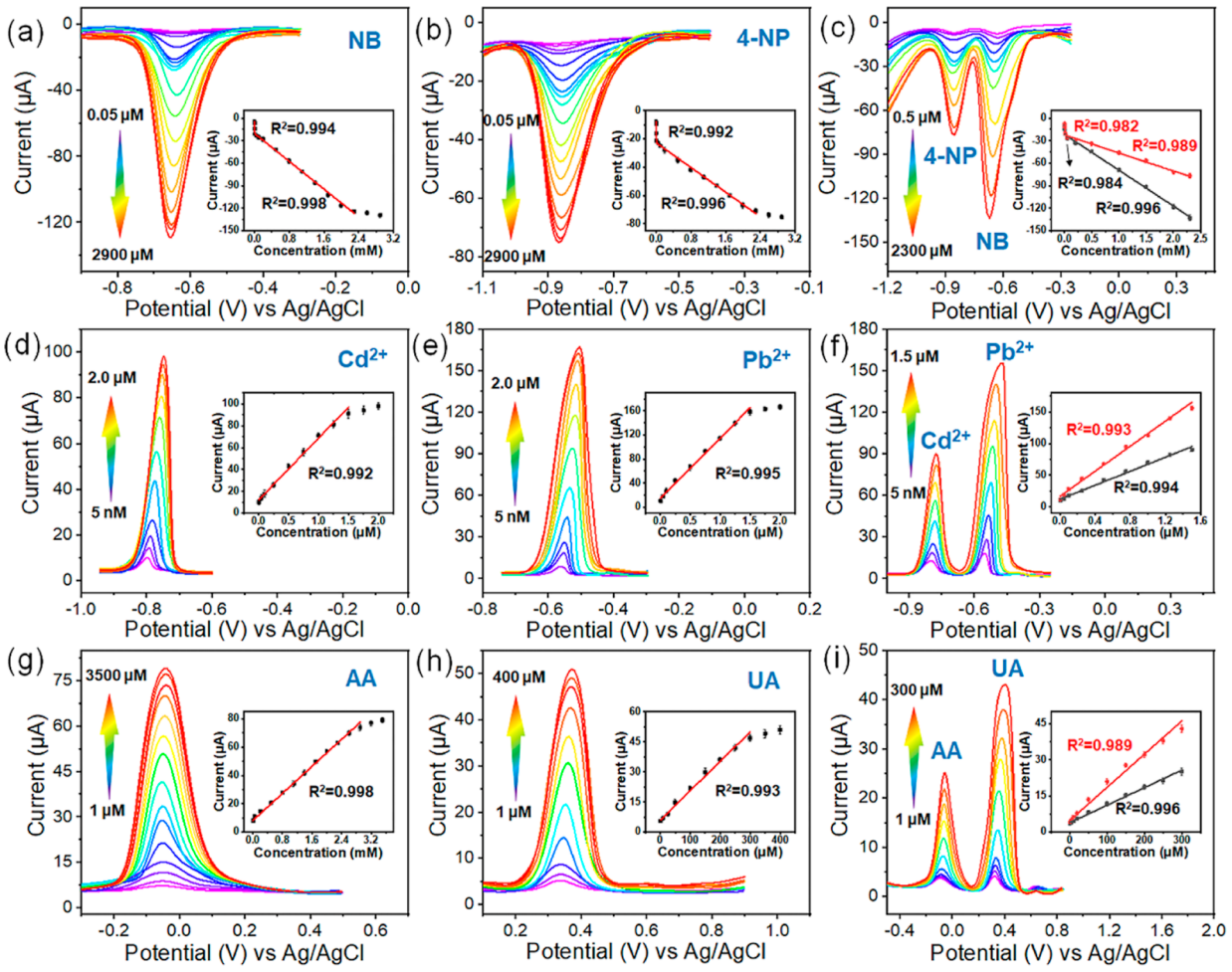

Figure 3. (a–c) DPV curves of GDY/G/GCE toward the detection of (a) NB, (b) 4-NP, and (c) NB and 4-NP. (d–f) DPASV curves of GDY/G/GCE toward the detection of (d) Cd^{2+}, (e) Pb^{2+}, and (f) Cd^{2+} and Pb^{2+}. (g–i) DPV curves of hemin/GDY/G/GCE toward the detection of (a) AA, (b) UA, and (c) AA and UA. The inset shows a linear trend of the peak current versus concentration of the corresponding analytes.

possesses the highest reduction peak currents toward NB, revealing the synergistic effect on current signal amplification after GDY payload on the graphene surface. Therefore, GDY/G/GCE is a promising electrochemical sensing platform for NB detection. The possible reasons for enhanced electrochemical response of GDY/G heterostructures to NB are as follows: the template function of graphene enables GDY to grow into a 2D ultrathin structure, which effectively overcomes the shortcoming of the poor conduction of bulk GDY. Few-layered GDY also provides more adsorption sites, which is conducive to the capture of detection signals. Moreover, graphene improves the charge conduction and finally ensures the efficient redox reaction.

3.5. Electrochemical Detection for NB and 4-NP. The feasibility of the GDY/G/GCE electrode for NB and 4-NP detection was examined under optimized conditions by adding different concentrations of NB and 4-NP (Figure 3a,b). Notably, as the NB and 4-NP concentrations increased, the corresponding reduction peak current also increased linearly. For individual detection, NB and 4-NP showed a two-stage linear relationship in the concentration range of 0.05–2300 μM: $y = -1.67x - 4.82$ (NB, 0.05–10 μM, $R^2 = 0.994$), $y = -0.046x - 20.41$ (NB, 10–2300 μM, $R^2 = 0.998$), $y = -1.49x - 7.53$ (4-NP, 0.05–10 μM, $R^2 = 0.992$), and $y = -0.022x - 22.73$ (4-NP, 10–2300 μM, $R^2 = 0.996$). The significant increase in sensitivity to low concentrations may be due to the following factors: (1) abundant catalytic sites at low concentrations are more likely to adsorb NB and 4-NP molecules; (2) these sites are sequestrated due to saturation with NB and 4-NP at higher concentrations, thus reducing sensitivity.[33,37] The limits of detection for NB and 4-NP are as low as 0.014 and 0.016 μM, respectively. Compared with the previously reported modified electrodes for NB and 4-NP detection, GDY/G/GCE exhibits low LOD and a wide linear detection range (Tables S1mand S2). The reasons for outstanding performance may be as follows: (1) the $\pi-\pi$ interaction between GDY and the benzene ring can facilitate the capture of NB and 4-NP. (2) The evenly distributed pores formed by 18 C atoms in GDY accelerate the transfer of materials and electrons.[41,42] According to previous reports, this kind of pore structure is helpful in distinguishing substances with a similar redox potential.[41] (3) The ultrathin GDY/G heterostructure effectively overcomes the shortcoming of a low electron collection efficiency of the thick GDY layer[31] and improves the specific surface area of the material, which provides more adsorption sites. Graphene also improves the conductivity of the electrode material. These characteristics of the GDY/G-modified electrode enable the redox reaction to be carried out efficiently.

https://doi.org/10.1021/acs.analchem.2c03387
Anal. Chem. 2022, 94, 13598–13606

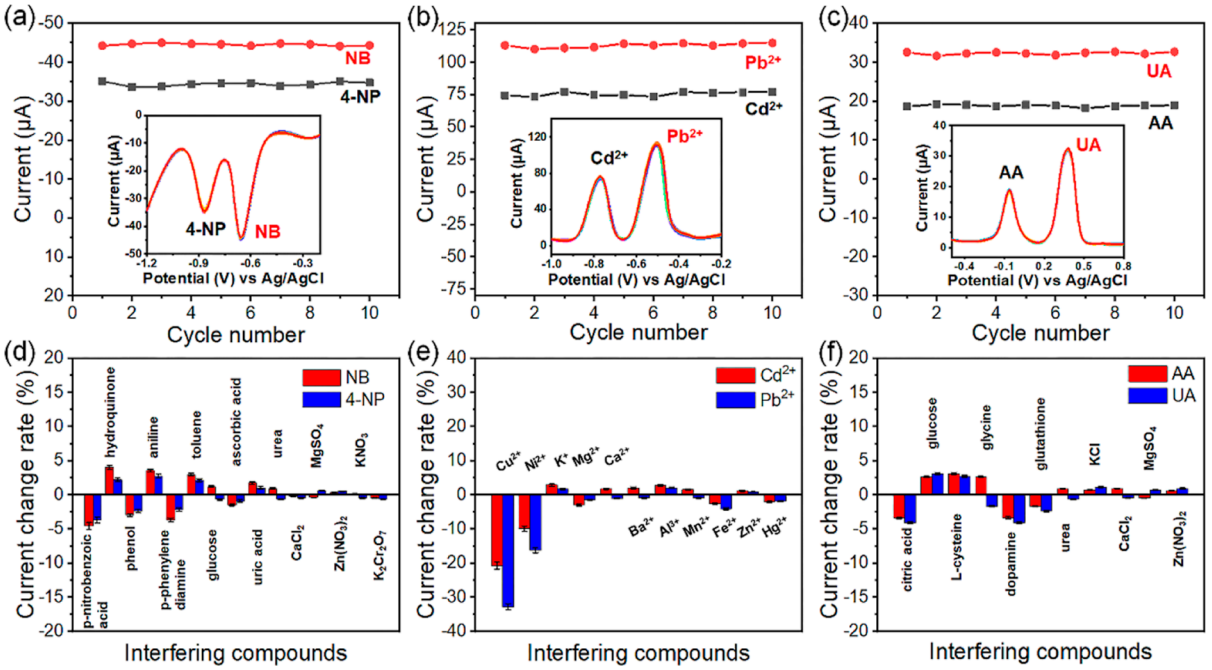

Figure 4. (a,b) Reproducibility of GDY/G/GCE. (a) 500 μM NB and 4-NP in pH 7.0, (b) 1 μM Cd^{2+} and Pb^{2+} in pH 5.0. (c) Reproducibility of hemin/GDY/G/GCE toward the detection of 200 μM AA and UA in pH 7.0. (d,e) Selectivity of GDY/G/GCE toward the detection of (d) NB and 4-NP and (e) Pb^{2+} and Cd^{2+}. (f) Selectivity of hemin/GDY/G/GCE toward the detection of AA and UA, each corresponding to additions of 5-fold of different interferents.

In addition to the detection of NB and 4-NP individually, the obtained GDY/G/GCE was successfully used for simultaneous electrochemical analysis of NB and 4-NP. Figure 3c shows the DPV response of the mixture of NB and 4-NP under optimal conditions. Evidently, for NB and 4-NP, two separate and well-resolved peaks are seen at 0.64 and 0.86 V, respectively. It is noted that the positions of the reduction peaks when NB and 4-NP coexist are almost unchanged with respect to their individual detection, indicating that the mutual interference between NB and 4-NP is very low. Due to the complete separation of the two peaks, the proposed GDY/G/GCE is anticipated to simultaneously identify NB and 4-NP. As expected, the reduction peak currents of NB and 4-NP also increased linearly with increasing NB and 4-NP concentrations. At the same time, NB and 4-NP have a good linear relationship in the range of 0.5−2300 μM, which can be evaluated as $y = -1.33x - 7.68$ (NB, 0.5−10 μM, $R^2 = 0.984$), $y = -0.048x - 21.71$ (NB, 10−2300 μM, $R^2 = 0.996$), $y = -1.25x - 6.79$ (4-NP, 0.5−10 μM, $R^2 = 0.982$), and $y = -0.024x - 22.3$ (4-NP, 10−2300 μM, $R^2 = 0.989$) for NB and 4-NP, respectively. Consequently, the LODs for NB and 4-NP are calculated to be 0.018 and 0.02 μM, respectively.

3.6. Electrochemical Detection for Pb^{2+} and Cd^{2+}. In view of its good response to electrical analysis, differential pulse anodic stripping voltammetry (DPASV) was used to quantitatively determine Pb^{2+} and Cd^{2+} of GDY/G-modified GCE. In order to determine the optimal condition of GDY/G/GCE to detect heavy metal ions, the effects of deposition time, pH, and deposition potential on the response current were studied (Figure S6). As shown in Figure 3d, when Cd^{2+} was detected individually, a clear peak was observed at about −0.8 V, which corresponds to the oxidation potential of cadmium. In addition, the relationship between Cd^{2+} concentration and stripping current was linear in the range of 0.005−1.5 μM. The linear equation is defined as $y = 56.61x + 12.11$ ($R^2 = 0.992$). Therefore, the LOD can be calculated to be 0.31 nM. Similarly, DPASV was used to investigate the response of GDY/G/GCE to Pb^{2+}. Figure 3e shows that there is a sharp peak at the potential of −0.56 V, which corresponds to the lead stripping peak. Additionally, in the range of 0.005−1.5 μM, the stripping current increased proportionally with the increase of Pb^{2+} concentration, and the linear relationship was as follows: $y = 100.42x + 14.5$ ($R^2 = 0.995$). Accordingly, the LOD was calculated to be 0.24 nM. Compared with previously reported modified electrodes for Pb^{2+} and Cd^{2+} detection, GDY/G/GCE has a lower LOD and a wide linear range (Tables S3 and S4). Compared with the $\pi-\pi$ interaction of organic pollutant detection, the excellent performance of heavy metal ion detection can be attributed to the following: (1) the acetylenic linkages of GDY are rich in π-electrons, making the surface of GDY more negative, which facilitates the approach of metal cations.[21,43] (2) The unique pore structure of GDY allows heavy metal ions to be embedded, providing an ideal adsorption location.[26,31]

As shown in Figure 3f, GDY/G/GCE also implements simultaneous detection of Pb^{2+} and Cd^{2+}. In the concentration range of 0.005−1.5 μM, the current response of GDY/G/GCE increases with the increase of Pb^{2+} and Cd^{2+} concentrations. The LODs can be calculated as 0.25 (Pb^{2+}) and 0.32 (Cd^{2+}) nM, respectively. Since the two peaks are completely separated and each shows a good linear relationship, the proposed GDY/G/GCE is likely to simultaneously identify Pb^{2+} and Cd^{2+}.

3.7. Electrochemical Detection for AA and UA. Hemin as a key enzyme catalytic motif was immobilized on GDY/G via $\pi-\pi$ interactions; details of the synthesis, characterization, and optimization of hemin/GDY/G are provided in the Supporting Information (Figures S7−S9). The electrode modified with hemin/GDY/G was successfully used for AA and UA detection. Figure 3g reveals the DPV curves of different AA concentrations. As the concentration of AA

https://doi.org/10.1021/acs.analchem.2c03387
Anal. Chem. 2022, 94, 13598−13606

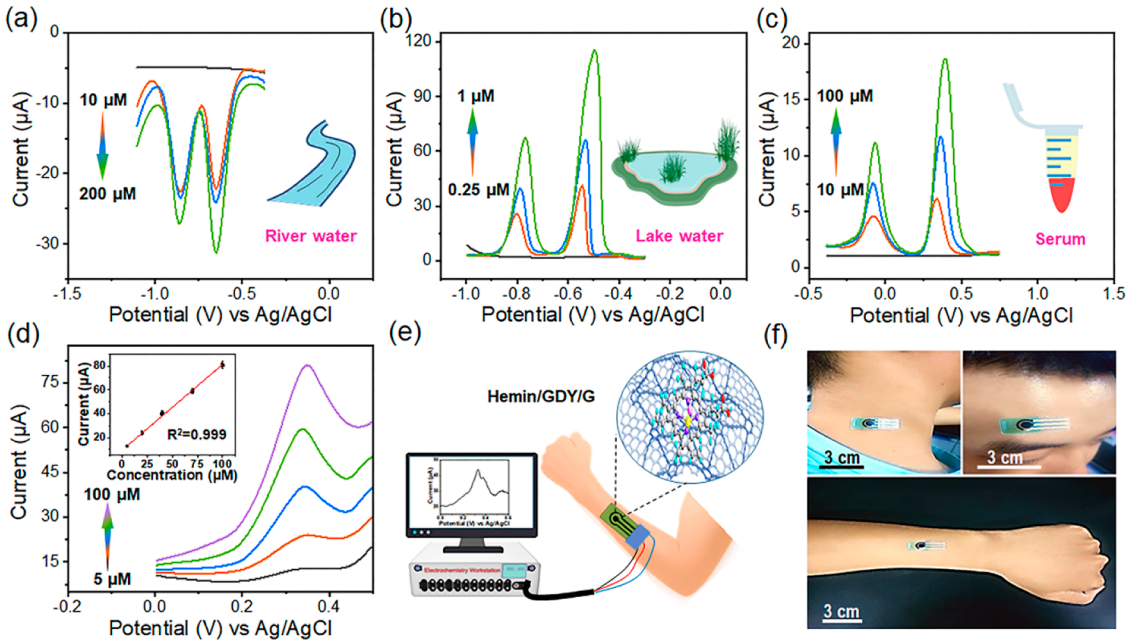

Figure 5. (a,b) Real sample analysis of GDY/G/GCE. (a) River water with different amounts of NB and 4-NP in pH 7.0. (b) Lake water with different amounts of Cd^{2+} and Pb^{2+} in pH 5.0. (c) Real sample analysis of hemin/GDY/G/GCE in serum with different amounts of AA and UA in pH 7.0. (d) DPV curves of different UA (5, 20, 40, 70, and 100 μM) concentrations at the hemin/GDY/G-modified screen-printed electrode. The inset shows the linear relationship between peak current and UA concentration. (e) Schematic diagram of the flexible and wearable sensor for UA sensing in human sweat. (f) Demonstration photos of the wearable biosensors attached on different parts of the body for monitoring.

increases from 1 to 2900 μM, the current response of the oxidation peak increases linearly at the potential of −0.052 V. The linear equation is described as $y = 0.024x + 8.23$ (R^2 = 0.998). The corresponding LOD is calculated to be 2.73 μM. Similarly, Figure 3h displays the peak current response increase linearly at the potential of 0.336 V with the UA concentration increasing from 1 to 300 μM. The linear equation is $y = 0.14x + 6.01$ (R^2 = 0.993). Accordingly, the LOD can be calculated to be 0.081 μM. To demonstrate the good performance of hemin/GDY/G/GCE, the linear range and LOD were compared with those of biosensors previously reported for AA and UA detection (Tables S5 and S6). It can be seen that the proposed biosensor has a low detection limit and a wide linear range.

For the simultaneous detection of AA and UA, Figure 3i shows the oxidation reaction of a mixture of AA and UA on hemin/GDY/G/GCE. The two well-defined voltammetric peaks observed correspond to the oxidation of AA and UA, respectively, and the peak currents increase with increasing concentrations of AA and UA. The results reveal that the hemin/GDY/G-modified sensor can accomplish the simultaneous detection of AA and UA.

3.8. Selectivity, Reproducibility, and Stability of Sensors. The stability and reproducibility are important factors of electrochemical sensors. GDY/G/GCE showed an excellent stability and retained 98.9, 98.6, 97.6, and 96.6% of initial response for NB, 4-NP, Pb^{2+}, and Cd^{2+} after 30 days, respectively (Figures S10a,b). Hemin/GDY/G/GCE retained 97.4 and 98.4% of initial response for AA and UA after 30 days, respectively (Figure S10c). Moreover, the stability after treatment with different temperatures (−20, 70 °C) was tested (Figure S11). It retained above 97% of the response at 25 °C for NB, 4-NP, Pb^{2+}, Cd^{2+}, AA, and UA; this is attributed to the high physical and chemical stability of the carbon material, that is, GDY and graphene.[44,45] Furthermore, the UV−vis spectra of hemin/GDY/G were compared (Figure S12). It was found that the modified electrode had the same molecular structure before and after continuous detection, indicating that hemin loaded on the GDY/G heterostructure had excellent stability.

Besides, to evaluate the repeatability of the proposed sensor, 10 experiments were repeated at the same electrode. As shown in Figure 4a,b GDY/G/GCE had satisfactory reproducibility (NB, RSD = 0.7%; 4-NP, RSD = 1.50%; Pb^{2+}, RSD = 1.48%; Cd^{2+}, RSD = 2.09%). At the same time, hemin/GDY/G/GCE also shows excellent reproducibility (AA, RSD = 1.48%; UA, RSD = 1.06%) (Figure 4c).

The selectivity of GDY/G/GCE was evaluated by adding a 5-fold molar amount of interferents to 200 μM NB and 4-NP solution (Figure 4d). It can be seen that the interference of common metal ions and biological species on the detection of NB and 4-NP is negligible (<2%), while benzene derivatives and phenolic compounds have only a slight influence in NB and 4-NP detection (<5%). These results indicate that the modified electrode can selectively detect NB and 4-NP even in the presence of excessive amounts of these potential interfering substances. The selectivity of GDY/G/GCE for Cd^{2+} and Pb^{2+} detection was also evaluated. A 5-fold molar amount of common metal ions was added to 1 μM Pb^{2+} and Cd^{2+} mixture solution with simultaneous detection to investigate the change of response current. As can be seen from Figure 4e, except Ni^{2+} and Cu^{2+}, the relative signal changes of other interfering ions are within the tolerance rate of ±5%, which means that the interference of non-target ions is small, demonstrating that GDY/G/GCE has high selectivity for Pb^{2+} and Cd^{2+} in the existence of other interfering ions. The interference of Cu^{2+} and Ni^{2+} was further studied, which may be due to the chemisorption interaction between GDY and Cu^{2+}/Ni^{2+} and the Cu−Pb interaction.[46−49] However, potassium ferrocyanide as a masking agent can reduce the interference of Cu^{2+} and Ni^{2+} (Figures S13a,b).[21] Furthermore, hemin/GDY/G/GCE

https://doi.org/10.1021/acs.analchem.2c03387
Anal. Chem. 2022, 94, 13598−13606

also showed excellent selectivity for AA and UA detection, with only slight interference (<5%) from several typical interferers, as shown in Figure 4f.

3.9. Real Sample Detection. To further evaluate the feasibility of the proposed sensor, NB and 4-NP in river water were detected using the modified electrode by adding different concentrations of NB and 4-NP (10, 50, and 200 μM), and three parallel measurements were performed at each concentration level (Figure 5a). As shown in Table S7, the detection of NB and 4-NP by GDY/G/GCE has excellent recoveries, and the RSD is less than 4.48%. In addition, samples were analyzed by high-performance liquid chromatography (HPLC) to verify the performance of the proposed sensor (Table S8). It can be seen that there is no significant difference between the two methods, indicating the reliability of the developed sensor. Similarly, the feasibility of testing for Pb^{2+} and Cd^{2+} in lake water (Figure 5b) and AA and UA in serum (Figure 5c) was evaluated. Compared with inductively coupled plasma mass spectrometry, HPLC, and colorimetry, the proposed sensor exhibits good recoveries and low RSDs.

Furthermore, hemin/GDY/G was modified on a commercial screen-printed electrode to monitor UA in human sweat to verify the feasibility of our electrochemical sensing platform as a wearable biosensor. As shown in Figure 5d, five UA standard solutions were measured, which are in a good linear correlation. Figure 5e is a schematic diagram of UA detection in human sweat. The sensor can be attached to different parts of the skin well to achieve the purpose of wearable detection (Figure 5f). Three samples were measured by using the modified screen-printed electrodes, and sweat was collected from different volunteers (24, 40, and 60 years). For comparison, UA concentration was determined using a commercial colorimetric assay kit. Since UA concentration is proportional to absorbance, the amount of UA in sweat was calculated from the standard curve (Figure S14a). As shown in Figure S14b, the results of the two analytical methods have good correlation, which shows that the sensing platform holds great potential in wearable biosensing.

4. CONCLUSIONS

In summary, the GDY/G 2D heterostructure was synthesized and employed for electrochemical detection of multiple targets. Compared with GDY, GDY/G shows a lower electrochemical impedance and a higher electrochemical active surface area, which are conducive to the diffusion of substances and electron transfer. GDY/G was used as a new electrode material in the electrochemical sensor, which shows high sensitivity for heavy metal ions (Pb^{2+}, Cd^{2+}) and toxic molecules (NB, 4-NP) due to the d−π and π−π interactions, respectively. Moreover, hemin as a key enzyme catalytic motif was immobilized on GDY/G via π−π interactions, and the sandwich structure of hemin/GDY/G was successfully utilized for AA and UA detection. Finally, the prepared electrode showed satisfactory recovery and RSD in real sample analysis, including waster and biological samples. In addition, the flexible and wearable UA sensor is also promising for the detection of UA in human sweat. This study demonstrates that GDY/G heterostructures can be used as a powerful electrochemical sensing platform for the detection of a wide range of environmental pollutants and medical diagnosis.

■ ASSOCIATED CONTENT

Supporting Information

The Supporting Information is available free of charge at https://pubs.acs.org/doi/10.1021/acs.analchem.2c03387.

Additional detailed experimental procedures, SEM of GDY, EIS of bare GCE, CV and DPV of the modified electrode, optimization of HEB content, optimization of heavy metal ion detection conditions, UV−vis and EDS characterization of hemin and hemin/GDY/G, hemin load ratio optimization, stability experiment, experiments with masking agents, standard curves of the UA assay kit, comparison of the UA colorimetric assay and electrochemical method, comparison of linear range and LOD with the literature, and real sample analysis (PDF)

■ AUTHOR INFORMATION

Corresponding Authors

Lina Wang − *College of Environment and Safety Engineering, Qingdao University of Science and Technology, Qingdao 266042, China*; Email: linawang@qust.edu.cn

Zhiling Zhu − *College of Materials Science and Engineering, Qingdao University of Science and Technology, Qingdao, Shandong 266042, China*; orcid.org/0000-0003-3878-0391; Email: zlzhu@qust.edu.cn

Ning Sui − *College of Materials Science and Engineering, Qingdao University of Science and Technology, Qingdao, Shandong 266042, China*; orcid.org/0000-0002-0543-8701; Email: suining@qust.edu.cn

Authors

Xiuchao Sun − *College of Materials Science and Engineering, Qingdao University of Science and Technology, Qingdao, Shandong 266042, China*

Menglu Duan − *College of Materials Science and Engineering, Qingdao University of Science and Technology, Qingdao, Shandong 266042, China*

Rongteng Li − *College of Materials Science and Engineering, Qingdao University of Science and Technology, Qingdao, Shandong 266042, China*

Yuan Meng − *College of Materials Science and Engineering, Qingdao University of Science and Technology, Qingdao, Shandong 266042, China*

Qiang Bai − *College of Materials Science and Engineering, Qingdao University of Science and Technology, Qingdao, Shandong 266042, China*

Manhong Liu − *College of Materials Science and Engineering, Qingdao University of Science and Technology, Qingdao, Shandong 266042, China*

Zhugen Yang − *School of Water, Energy and Environment, Cranfield University, Milton Keynes MK43 0AL, United Kingdom*; orcid.org/0000-0003-4183-8160

Complete contact information is available at: https://pubs.acs.org/10.1021/acs.analchem.2c03387

Notes

The authors declare no competing financial interest.

■ ACKNOWLEDGMENTS

The authors acknowledge the National Natural Science Foundation of China (31800800, 21501106) and the Natural Science Foundation of Shandong Province China (ZR2019BC101, ZR2020MB026, ZR202103010467).

REFERENCES

(1) Hu, W.; Chang, Y.; Huang, J.; Chai, Y.; Yuan, R. *Anal. Chem.* **2022**, *94*, 6860−6865.
(2) Banga, I.; Paul, A.; Muthukumar, S.; Prasad, S. *ACS Appl. Mater. Interfaces* **2021**, *13*, 16155−16165.
(3) Wang, C.; Li, J.; Kang, M.; Huang, X.; Liu, Y.; Zhou, N.; Zhang, Z. *Anal. Chim. Acta* **2021**, *1141*, 110−119.
(4) Wu, L.; Gao, J.; Lu, X.; Huang, C.; Dhanjai; Chen, J. *Carbon* **2020**, *156*, 568−575.
(5) Kokulnathan, T.; Wang, T.-J.; Ashok Kumar, E.; Ahmed, F. *Chem. Eng. J.* **2022**, *433*, 133639.
(6) Lin, M.; Wan, H.; Zhang, J.; Wang, Q.; Hu, X.; Xia, F. *ACS Appl. Mater. Interfaces* **2020**, *12*, 45814−45821.
(7) Suhito, I. R.; Kim, J. W.; Koo, K.-M.; Nam, S. A.; Kim, Y. K.; Kim, T.-H. *Adv. Sci.* **2022**, *9*, 2200074.
(8) Wu, N.; Jiao, L.; Song, S.; Wei, X.; Cai, X.; Huang, J.; Sha, M.; Gu, W.; Song, W.; Zhu, C. *Anal. Chem.* **2021**, *93*, 15982−15989.
(9) Fu, C.; Yi, D.; Deng, C.; Wang, X.; Zhang, W.; Tang, Y.; Caruso, F.; Wang, Y. *Chem. Mater.* **2017**, *29*, 5286−5293.
(10) Chen, Y.; Liu, B.; Chen, Z.; Zuo, X. *Anal. Chem.* **2021**, *93*, 10635−10643.
(11) Dau, T. N. N.; Vu, V. H.; Cao, T. T.; Nguyen, V. C.; Ly, C. T.; Tran, D. L.; Pham, T. T. N.; Loc, N. T.; Piro, B.; Vu, T. T. *Sens. Actuators, B* **2019**, *283*, 52−60.
(12) Huang, L.; Chen, H.; Diao, D. *Anal. Chim. Acta* **2022**, *1198*, 339527.
(13) Prakash, J.; Dey, A.; Uppal, S.; Alexander, R.; Kaushal, A.; Misra, H. S.; Dasgupta, K. *Biosens. Bioelectron.* **2021**, *191*, 113480.
(14) Bi, Y.; Hei, Y.; Wang, N.; Liu, J.; Ma, C.-B. *Anal. Chim. Acta* **2021**, *1164*, 338514.
(15) Guo, S.; Yan, H.; Wu, F.; Zhao, L.; Yu, P.; Liu, H.; Li, Y.; Mao, L. *Anal. Chem.* **2017**, *89*, 13008−13015.
(16) Zhou, J.; Li, J.; Liu, Z.; Zhang, J. *Adv. Mater.* **2019**, *31*, 1803758.
(17) Bai, Q.; Luo, H.; Yi, X.; Shi, S.; Wang, L.; Liu, M.; Du, F.; Yang, Z.; Sui, N. *Microchem. J.* **2022**, *179*, 107521.
(18) Cui, J.; Liu, J.; Wang, C.; Rong, F.; He, L.; Song, Y.; Zhang, Z.; Fang, S. *Electrochim. Acta* **2020**, *334*, 135577.
(19) Chauhan, D.; Kumar, Y.; Chandra, R.; Kumar, S. *Biosens. Bioelectron.* **2022**, *213*, 114433.
(20) Hou, Y.-Y.; Xu, J.; Wang, F.-T.; Dong, Z.; Tan, X.; Huang, K.-J.; Li, J.-Q.; Zuo, C.-Y.; Zhang, S.-Q. *Anal. Chem.* **2021**, *93*, 15225−15230.
(21) Li, Y.; Huang, H.; Cui, R.; Wang, D.; Yin, Z.; Wang, D.; Zheng, L.; Zhang, J.; Zhao, Y.; Yuan, H.; Dong, J.; Guo, X.; Sun, B. *Sens. Actuators, B* **2021**, *332*, 129519.
(22) Niu, K.; Gao, J.; Wu, L.; Lu, X.; Chen, J. *Anal. Chem.* **2021**, *93*, 8656−8662.
(23) Shi, M.; Sun, X.; Bai, Q.; Zhang, Y.; Yu, S.; Liu, M.; Wang, L.; Yu, W. W.; Sui, N. *Colloids Surf., A* **2022**, *637*, 128217.
(24) Gao, X.; Zhu, Y.; Yi, D.; Zhou, J.; Zhang, S.; Yin, C.; Ding, F.; Zhang, S.; Yi, X.; Wang, J.; Tong, L.; Han, Y.; Liu, Z.; Zhang, J. *Sci. Adv.* **2018**, *4*, No. eaat6378.
(25) Li, J.; Yi, Y.; Zuo, X.; Hu, B.; Xiao, Z.; Lian, R.; Kong, Y.; Tong, L.; Shao, R.; Sun, J.; Zhang, J. *ACS Nano* **2022**, *16*, 3163−3172.
(26) Li, J.; Zhong, L.; Tong, L.; Yu, Y.; Liu, Q.; Zhang, S.; Yin, C.; Qiao, L.; Li, S.; Si, R.; Zhang, J. *Adv. Funct. Mater.* **2019**, *29*, 1905423.
(27) Gu, H.; Zhong, L.; Shi, G.; Li, J.; Yu, K.; Li, J.; Zhang, S.; Zhu, C.; Chen, S.; Yang, C.; Kong, Y.; Chen, C.; Li, S.; Zhang, J.; Zhang, L. *J. Am. Chem. Soc.* **2021**, *143*, 8679−8688.
(28) Zhang, Q.; Bai, Q.; Cai, E.; Hao, L.; Wang, M.; Zhang, S.; Zhao, Q.; Teng, L.; Sui, N.; Du, F.; Wang, X. *Results Phys.* **2022**, *38*, 105654.
(29) Wang, J.; Yu, P.; Kan, K.; Lv, H.; Liu, Z.; Sun, B.; Bai, X.; Chen, J.; Zhang, Y.; Shi, K. *Chem. Eng. J.* **2021**, *420*, 130317.
(30) Ma, Y.; Wang, Y.; Xie, D.; Gu, Y.; Zhu, X.; Zhang, H.; Wang, G.; Zhang, Y.; Zhao, H. *Chem. Eng. J.* **2018**, *347*, 953−962.
(31) Lv, Y.; Wu, X.; Lin, H.; Li, J.; Zhang, H.; Guo, J.; Jia, D.; Zhang, H. *Small* **2021**, *17*, 2006442.
(32) Biswas, S.; Chen, Y.; Xie, Y.; Sun, X.; Wang, Y. *Anal. Chem.* **2020**, *92*, 4566−4572.
(33) Chen, Y.; Sun, X.; Biswas, S.; Xie, Y.; Wang, Y.; Hu, X. *Biosens. Bioelectron.* **2019**, *141*, 111470.
(34) Wang, Y.; Wang, L.; Chen, H.; Hu, X.; Ma, S. *ACS Appl. Mater. Interfaces* **2016**, *8*, 18173−18181.
(35) Wang, Y.; Wang, L.; Huang, W.; Zhang, T.; Hu, X.; Perman, J. A.; Ma, S. *J. Mater. Chem. A* **2017**, *5*, 8385−8393.
(36) Yang, J.; Gunasekaran, S. *Carbon* **2013**, *51*, 36−44.
(37) Zhou, Z.; Mukherjee, S.; Hou, S.; Li, W.; Elsner, M.; Fischer, R. A. *Angew. Chem., Int. Ed.* **2021**, *60*, 20551−20557.
(38) Zhu, W.; Gao, J.; Song, H.; Lin, X.; Zhang, S. *ACS Appl. Mater. Interfaces* **2019**, *11*, 44545−44555.
(39) Gao, J.; Liu, M.; Song, H.; Zhang, S.; Qian, Y.; Li, A. *J. Hazard. Mater.* **2016**, *318*, 99−108.
(40) Gao, J.; Fang, J.; Ju, X.; Zhu, W.; Lin, X.; Zhang, S.; Ma, C.; Song, H. *ACS Appl. Mater. Interfaces* **2017**, *9*, 38802−38813.
(41) Zhang, Y.; Xie, Q.; Xia, Z.; Gui, G.; Deng, F. *J. Electroanal. Chem.* **2020**, *863*, 114058.
(42) Nan, D.; Huang, Z.-H.; Lv, R.; Yang, L.; Wang, J.-G.; Shen, W.; Lin, Y.; Yu, X.; Ye, L.; Sun, H.; Kang, F. *J. Mater. Chem. A* **2014**, *2*, 19678−19684.
(43) Guo, X.; Li, Y.; Huang, H.; Wang, D.; Cui, R.; Li, J.; Zhao, Y.; Wang, D.; Yuan, H.; Dong, J.; Sun, B. *J. Environ. Chem. Eng.* **2022**, *10*, 107159.
(44) Poletti, F.; Scidà, A.; Zanfrognini, B.; Kovtun, A.; Parkula, V.; Favaretto, L.; Melucci, M.; Palermo, V.; Treossi, E.; Zanardi, C. *Adv. Funct. Mater.* **2022**, *32*, 2107941.
(45) Niu, K.; Zuo, Z.; Lu, X.; Zou, L.; Chen, J. *Biosens. Bioelectron.* **2022**, *205*, 114111.
(46) Zhai, Z.; Huang, N.; Zhuang, H.; Liu, L.; Yang, B.; Wang, C.; Gai, Z.; Guo, F.; Li, Z.; Jiang, X. *Appl. Surf. Sci.* **2018**, *457*, 1192−1201.
(47) Mashhadzadeh, A. H.; Vahedi, A. M.; Ardjmand, M.; Ahangari, M. G. *Superlattices Microstruct.* **2016**, *100*, 1094−1102.
(48) He, J.; Wang, N.; Yang, Z.; Shen, X.; Wang, K.; Huang, C.; Yi, Y.; Tu, Z.; Li, Y. *Energy Environ. Sci.* **2018**, *11*, 2893−2903.
(49) Sun, M.; Wu, T.; Xue, Y.; Dougherty, A. W.; Huang, B.; Li, Y.; Yan, C.-H. *Nano Energy* **2019**, *62*, 754−763.

https://doi.org/10.1021/acs.analchem.2c03387
Anal. Chem. 2022, 94, 13598−13606